

*Scientific Paper*Doi: <http://dx.doi.org/10.1590/1809-4430-Eng.Agric.v43n2e20220127/2023>**STUDY ON TILLAGE RESISTANCE AND ENERGY CONSUMPTION OF A PLAIN STRAIGHT ROTARY BLADE FOR STRIP TILLAGE****Yiwen Yuan¹, Jiayi Wang², Xin Zhang³, Shuhong Zhao^{1*}**

^{1*}Corresponding author. College of Engineering, Northeast Agricultural University/Harbin, China.
E-mail: shhzh@neau.edu.com | ORCID ID: <https://orcid.org/0000-0001-6146-3541>

KEYWORDS

tillage resistance,
power consumption,
fuel consumption,
torque,
DEM-CFD.

ABSTRACT

The issue of reducing tillage resistance and lowering energy consumption has become increasingly relevant. Strip tillage has a positive impact on soil protection and energy consumption reduction. This study analysed the tillage resistance components of rotary blades and their relationship with operating parameters and developed a mathematical relationship between tillage resistance and energy consumption (power and fuel consumption). We summarised tillage resistance into three parts: air resistance, lateral rotational friction resistance (divided into horizontal and vertical resistance), and shear force. By theoretical analysis and coupled simulation tests 11 (DEM-CFD), we obtained an air resistance, lateral rotational friction, and shear force of 0.0883 N, 97.21 N, and 893.496 N, respectively, accounting for 0.01%, 9.81%, and 90.18% of tillage resistance. Meanwhile, we found that horizontal resistance decreased linearly with the increase of angular speed, which was the opposite of vertical resistance. Horizontal and vertical resistance increased linearly with the increase in contact area. Shear force increased significantly with angular speed. Fuel consumption in the field test and tillage resistance and power consumption in coupled simulation was formed to build a correspondence point, and a mathematical relationship between tillage resistance, torque, and power and fuel consumption was established.

INTRODUCTION

Strip tillage, the procedure of planting seed into narrow furrows and limiting soil inversion, is relatively new, having been evaluated for the first time in the early 1990s (Celik et al., 2013). This operation mode confines tillage to a narrow strip where the crop will be planted (Luna & Staben, 2002) and divides the cropping system into two distinct adjacent zones: tilled and untilled (Lowry et al., 2021). Within the crop row, tillage can provide a finer seedbed (Licht & Al-Kaisi, 2005), while the untilled zone between rows maintains no-tilled states. It combines the benefits of both conservation agriculture and conventional tillage. Compared to conventional tillage, strip tillage offers greater crop yields at reduced production costs and better soil erosion control (Laufer & Koch, 2017). The tilled zone enhances soil water evaporation and

seedbed warming, while minimising total soil disturbance (Licht & Al-Kaisi, 2005). It offers a potential solution to late seed emergence due to cool and wet soil conditions associated with no tillage (Turmel et al., 2015). Strip tillage is preferable for proper seedbed preparation compared to direct drilling because it creates favourable conditions for seed germination; in comparison with full tillage, it reduces the working time and fuel and production costs, protects soil, and is ecologically benign (Vaitauskienė et al., 2017).

The improvement of operational efficiency has been a subject of considerable research. Operation efficiency can be improved by reducing tillage resistance and lowering energy consumption. The rotary blade is the core soil-engaging tool of the soil preparation machine for strip tillage (Saimbhi et al., 2004). Tillage resistance, the

¹ College of Engineering, Northeast Agricultural University/Harbin, China.

² Weichai Lovol Heavy Industry CO., Ltd./Weifang, China.

³ Heilongjiang Academy of Agricultural Machinery Engineering Sciences/Harbin, China.

Area Editor: Fábio Lúcio Santos

Received in: 8-9-2022

Accepted in: 3-28-2023

most important indicator to assess the operational efficiency of tools for soil cultivation in plant production has been one of the crucial issues for rotary blades in the first two decades of the 21st century (Ahmadi, 2018; Asl & Singh, 2009; Tong et al., 2015). The main research results during this period include the proposed method of resistance reduction for contact parts and the investigation of the relationship between resistance and its affecting factors. Vibration resistance reduction (Shahgoli et al., 2009, 2010), bionic resistance reduction (Guan et al., 2022; Yang et al., 2018; Zhang et al., 2014), layered resistance reduction (Kasisira & du Plessis, 2006), structural design resistance reduction (Kichler et al., 2011), surface coating resistance reduction (Foley et al., 1984; Guan et al., 2021), etc., and the relationship between indexes and factors under each method theory is constantly evolving. Reece (1965) was the first to suggest the general earth pressure model, which has since been widely used by almost all researchers attempting to predict soil cutting resistance. McKyes & Desir (1984) used the equilibrium mechanics technique to describe soil resistance as a function of the failure angle β , soil characteristics, and tool parameters. Zhang & Kushwaha (1995) considered soil cutting resistance to be dependent on the failure shape and pattern. The problems of identification of the working resistance of soil-engaging tools in all directions have been the subject of many studies. Kogut et al. (2016) investigated horizontal, longitudinal, and vertical components of working resistance of a compact disc harrow. In the analysis of the resistance mechanism of the rotary blade, the pressure and cutting force of the component cutting into the soil are the main objects of analysis, ignoring the resistance generated by other parts of the component. There is no perfect system of resistance for all parts of the soil-engaging components. In the rotary operation process, blade rotation and the surrounding air form friction, impact; blade lateral extrusion by the soil; blade and soil to form shear. These constitute the tillage resistance of the rotary blade. Therefore, the construction of a complete set of rotary blade tillage resistance theories will make the design and research of rotary blades more clear.

Energy, as power and fuel consumption, is proportional to tillage resistance under cultivation. Soil tillage resistance is too large and will inevitably lead to high energy consumption, affecting the cost of agricultural production, intensifying the loss of machinery, and reducing operational efficiency. Thus, energy consumption has become an important indicator to evaluate the merits of tillage tools. Therefore, carrying out research on energy consumption in agricultural production is an effective means to promote the high quality and efficient development of agricultural mechanisation and has important practical value and significance for sustainable agricultural development. Part of the energy consumption is used to overcome tillage resistance. Numerous studies have measured the draught, power requirement, and fuel consumption of tillage equipment (Al-Janobi, 2000; Sahu & Raheman, 2006; Serrano et al., 2003, 2007). Predicting tractor fuel consumption may result in more prudent tractor

management choices. Ahmadi (2017) constructed rotational power prediction equations based on the classical laws of mechanics with an average error of 16% and 5% compared to the results of Asl & Singh (2009) and Chertkiattipol & Niyamapa (2010), respectively. Matin et al. (2015) analysed conventional, half-width, and straight-edge rotary blades at different rotational speeds for torque, power, and energy consumption characteristics at different rotational speeds, pointing out that peak torque occurs further back in phase as the rotational speed increases. In summary, most of the existing literature is based on theoretical predictions of energy consumption or studies of the effects of different parameters on energy consumption. A mathematical relationship model between tillage resistance, power, and fuel consumption has not been established to provide a basis for the study of resistance and energy consumption reduction.

The discrete element approach has made significant strides in the area of soil cultivation in recent years, and discrete element simulation modelling has been used to investigate the interaction between soil and equipment (Azimi-Nejadian et al., 2022; Li et al., 2014; Mak & Chen, 2015). Computational fluid dynamics (CFD) has also become a popular and highly valued engineering technology among agricultural researchers for simulating fluid flow, describing flow fields, and identifying fluid phase mechanisms for sustainable development (Lee et al., 2022; Teitel et al., 2022; Zhao et al., 2012). To describe detailed dynamic information, including particle velocity, instantaneous forces acting on each particle, airflow, and interactions between gas and solid phases, discrete element method and computational fluid dynamics (DEM-CFD) techniques have been coupled (Chen et al., 2022; Kong et al., 2022; Sakai & Koshizuka, 2009). In this study, the purpose of forming a flow field by simulating the high-speed rotation of blades in the EDEM can be achieved by the DEM-CFD coupling method. In this way, the airflow can be considered in the discrete element simulation to make the simulation results more realistic.

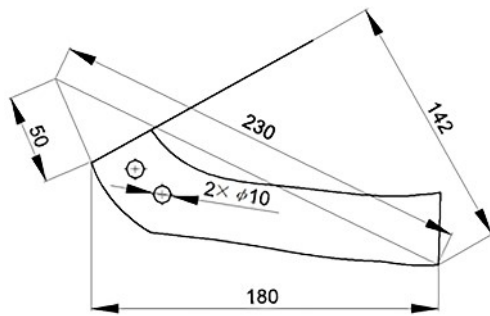
Of the two types of blades applied in strip rototillers, plain straight blades are more compatible with conservation tillage to reduce soil disturbance than bent blades that cause excessive soil loss in the furrow zone (Matin et al., 2021). The plain straight blade, which has only a lengthwise section (Matin et al., 2014), has been adopted by several researchers (Matin et al., 2015, 2016) to replace traditional blades because, under certain circumstances, this blade causes less soil disturbance and reduces fuel consumption. This study analysed the composition of tillage resistance and its relationship with operating parameters, and established a mathematical relationship model between tillage resistance, torque, and fuel consumption to provide a corresponding reference for the study of resistance and consumption reduction of driving rotary blades.

MATERIAL AND METHODS

Test scheme of tillage resistance

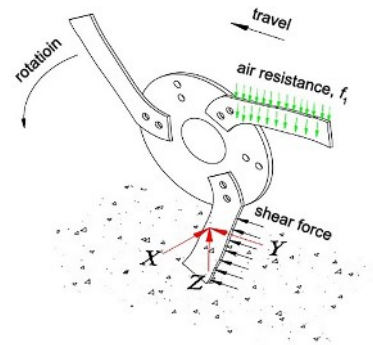
A plain straight rotary blade used for strip tillage

was evaluated in this study, as shown in Fig. 1a. Based on the field operation conditions of the plain straight rotary blade, the causes of its tillage resistance were meticulously divided and studied; its force state is shown in Fig. 1b.



a. Geometric parameters of blade

Tillage resistance of the rotary blade was generated by three parts: air resistance, lateral angular friction resistance (divided into lateral horizontal resistance and vertical resistance), and shear force.



b. Force principle diagram of plain straight rotary blade during operation

FIGURE 1. The plain straight rotary blade used in this research institute.

Friction and impact were formed by blade rotation and air; the blade was laterally squeezed by soil; shearing was produced by the cutting of the blade against the soil. The friction and impact between the air and the blade were defined as air resistance (f_1). The lateral extrusion of the blade was defined as the lateral pressure (X). The resistance formed by the lateral pressure was defined as the horizontal resistance (Y) and the vertical resistance (Z), both of which constituted the lateral rotational friction resistance of the plain straight rotary operation. The shear of the blade edge was defined as the shear force (F_t), and these three parts constitute the tillage resistance of the rotary blade.

Air resistance

The air resistance was mainly the interaction with the air during the high-speed rotation of the rotary blade. During operation, air resistance was calculated as follows (Kravchenko et al., 2019):

$$f_1 = \frac{1}{2} C \rho S v^2 \tag{1}$$

where:

- f_1 is air resistance, N;
- C is air resistance coefficient, $C=0.3$;
- ρ is air density, $\text{kg}\cdot\text{m}^{-3}$, $\rho=1.293 \text{ kg}\cdot\text{m}^{-3}$;
- S is windward area of the object, mm^2 ,
- v is the relative velocity of an object to air, $\text{m}\cdot\text{s}^{-1}$.

Therefore, air resistance was jointly influenced by the air resistance coefficient, air density, relative velocity, and target area. Combined with the blade size, the target area S was 5436 mm^2 . The relative velocity v between the object and air was the average linear velocity of blade rotation. The relative velocity of [eq. (2)] is given by:

$$v = \omega R \tag{2}$$

where:

- ω is the angular speed of the rotary blade at the high output shaft position of tractor;
- $\omega=75.36 \text{ rad}\cdot\text{s}^{-1}$ (i.e., tractor high-grade output shaft knife roller speed, 720 rpm),
- R is the average radius, $R=165 \text{ mm}$.

Therefore, the relative velocity of an object to air v was $12.4344 \text{ m}\cdot\text{s}^{-1}$, and the result was that the air resistance of the rotary blade was 0.0815 N .

Lateral rotational friction

During the soil cutting operation, the movement of the blade was idealised as a planar movement (with the tractor's translation accompanied by rotation around the rotor); therefore, the resulting lateral rotational friction was different from the planar sliding friction in the current study. The main operating parameters associated with the planar motion of the rotating blade were the rotational angular speed of the blade and the contact area with the soil and straw. To ensure the stability of the test environment, discrete element software EDEM 2018™ was used to carry out the simulation test.

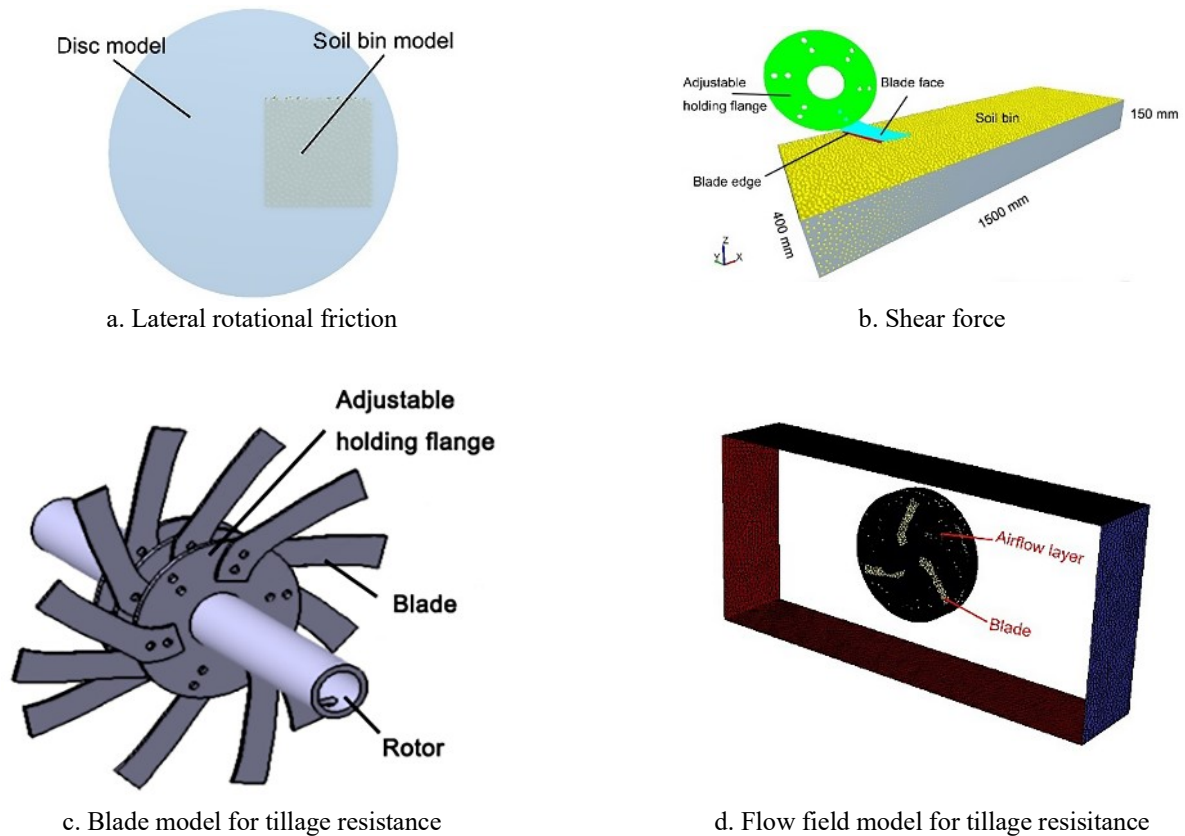


FIGURE 2. Simulation model of tillage resistance in each part of the rotary blade.

In the simulation test, to investigate the relationship between the lateral rotational friction and the angular speed of the blade in plane motion, the angular speed was simulated by setting the kinetic parameters of the blade. The contact area was changed by enlarging the blade model and shrinking the soil and straw models to achieve a change in contact area. To make the model in the experimental investigation more stable, this part of the soil and straw model was simplified to a soil bin model, requiring the moving parts to be able to achieve rotation and translation; thus, the blade model was idealised as an enlarged disc model, as shown in Fig. 2a.

The disc (500 mm in diameter) and soil bins of different cross-sectional area sizes were established. To avoid the disc model from moving without detaching from the soil bins, the soil bins were reduced in size and established with Y (horizontal) \times Z (vertical) \times X (lateral) of $60 \times 60 \times 60$, $100 \times 100 \times 60$, $120 \times 120 \times 60$, and $150 \times 150 \times 60$ mm³. The cross-sectional area of the soil bin was smaller than the area of the disc, so that when the disc model moved, the soil bin model was located on the side of the disc model.

The disc forward speed was set to 0.56 m·s⁻¹. The disc angular speed was set to 56.52 and 75.36 rad·s⁻¹

(tractor low-grade output shaft knife roller speed), as well as 0 , 28 , and 84 rad·s⁻¹ (equal spacing single-factor probe). The starting position of each movement of the disc did not cause the soil to break away from the disc model. Each group of tests was repeated three times, and the average value was used for the evaluation criteria. The points with large differences were excluded.

The pressure in the X -axis and Y -axis directions was extracted in the post-processing module to obtain lateral pressure and horizontal resistance, respectively. Since the vertical resistance of the blade was in opposite directions during soil entry and exit, the vertical resistance of the disc in model exploration consisted of the resistance generated by the blade cutting into soil and leaving soil (separated by the centre line, rotating clockwise, and moving to the right), as shown in Fig. 3, but the vertical resistance was mainly determined by the entry resistance because the disc was less extruded from the lateral soil particles during the exit process. The blade operation process involved both incoming and outgoing blades, and the overall incoming and outgoing resistance was obtained by extracting the resistance in the Z -axis direction in the post-processing module and summing them in reverse order.



FIGURE 3. Vertical resistance schematic.

Shear force

The shear force determines the operational effectiveness of the rotary blade. To avoid the influence of the resistance generated by other parts on the test results and the requirement to control the stability of the test environment, this part was implemented in the discrete element software. A single plain straight rotary blade model was established, and the blade and the adjustable holding flange were established as an assembly (blade edge and blade face were set as two parts), and only the resistance of the blade edge part was extracted, i.e., the shear force. The simulation model is shown in Fig. 2b, and the simulation parameters were the same as the soil parameter, as shown in Table 1. The shear force of the blade edge in the x-axis direction was extracted in the post-processing module, and blade resistance was extracted to obtain the shear force and the tillage resistance of the individual blade operation process.

Tillage resistance

According to the actual field operation of the driven rotary blade, the blade assembly model was assembled as the rotary blade model in Fig. 2c, and the airflow–soil–blade coupling field with discrete elements and finite elements was established, and the operating parameters were consistent with the normal operation in the field, with a forward speed of $0.56 \text{ m}\cdot\text{s}^{-1}$ and an angular speed of $75.36 \text{ rad}\cdot\text{s}^{-1}$. The motion mode was set as rotation accompanied by translation, and the total motion time was 1 s. The air resistance, lateral rotational friction, and shear force data were extracted in the post-processing module of EDEM 2018TM.

Energy consumption

Based on the coupled simulation test in section **Tillage resistance**, the dynamic tillage resistance and torque of rotary blade operation were extracted, and the results were output in the Analyst module of EDEM 2018TM. The corresponding power consumption was calculated and output. The obtained data were imported into Matlab 2014a, and the mathematical relationship models of tillage resistance, torque, and power consumption were established.

The fuel consumption of rotary blade operation could not be obtained in the simulation test. To obtain fuel consumption, the field test was conducted at the research farm ($44^{\circ} 04' - 46^{\circ} 40' \text{N}$ and $125^{\circ} 42' - 130^{\circ} 10' \text{E}$) of Northeast Agricultural University located in Heilongjiang Province of north-eastern China with an area

of 0.4 hm^2 from November 3–6, 2020. This region has a typical temperate continental monsoon climate and shows the continental climate with a short hot period during summer and a long cold period during winter. The mean annual precipitation is 569.1 mm, and more than 60% of the precipitation occurs from June to September. The average annual potential evapotranspiration is 1009 mm (1971–2000) and markedly exceeds the annual precipitation. Soil in the northeast is typically black soil (Typic Hapludoll, USDA, 1993) with a clay loam texture containing 36.0% sand, 24.5% silt, and 39.5% clay (Zhang et al., 2015). The distance between two adjacent ridges was 650 mm. The average moisture content of soil was 20.4%.

A single test rotor, as shown in Fig. 2c, was fitted with twelve blades (Fig. 1a). A double row rotary tillage implement fitted with two rotor assemblies were pulled by a Benye 454 Tractor (Ningbo Benye Tractor & Automobile Manufacturing Co., Ltd.). The test measurements were power consumption and fuel consumption. The power consumption was measured using a power sensor, which was installed behind the engine output shaft. The fuel consumption was measured by a fuel consumption measuring instrument, which was installed between the tank and the bottom of the injection pump. The sensors and fuel consumption measuring instrument were connected to the GPS-10A motor vehicle multifunction tester, which was installed on the tractor. The forward travel and angular speed of the rotor were constant at $0.56 \text{ m}\cdot\text{s}^{-1}$ and $75.36 \text{ rad}\cdot\text{s}^{-1}$ (equivalent to the rotation speed of the high-grade output shaft of the tractor), respectively. During operation, the tractor's power consumption and fuel consumption were monitored by the motor vehicle multifunction tester. Each test area was divided into a test area of 10 m and a preparation area of 5 m. The machine entered the test area after reaching a smooth speed in the test preparation area, and each test was repeated three times, with the average value as the evaluation standard for each test. The results of power consumption and fuel consumption were the average values of the 10 m operation process. The data output for the steady state of the whole tractor operation process, and the data corresponding to the coupled simulation time step, was selected in the steady state for collation. Power consumption in the field test was compared with that in the coupled simulation test to further verify the reliability of the coupled simulation model and to establish a mathematical relationship between tillage resistance and torque in the coupled simulation test and fuel consumption in the field test.

Simulation model development and parameters

The contact model is an essential basis of the discrete element method, which in essence is the result of contact mechanics elastoplastic analysis of granular solids under quasi-static conditions. The analytical calculation of the contact model directly determines the magnitude of the forces and moments applied to the particles, which in turn determines the trajectory of the particles during the est. To improve the accuracy of the simulation results, different contact types must be established for different simulation objects.

To describe the cohesion of agricultural soils, in addition to the Hertz–Mindlin (no slip) contact model between soil particles (Aleshin & Van Den Abeele, 2009; de Billy & Cohen Tenoudji, 2021; Wang et al., 2020), considering the strong cohesion properties between loam

and the mutual bonding between soils, the Hertz–Mindlin with Bonding contact model was added (Shaikh et al., 2021; Su et al., 2020; Wang et al., 2019). Virtual soil bin models were created using clay loam particles with an 8-mm radius (selected based on available computation time), and soil particles were randomly generated and settled to reach an equilibrium state in the soil bin.

A three-dimensional model of the rotary blade (with a density of $7865 \text{ kg}\cdot\text{m}^{-3}$) was established in Catia V5 software and then imported into the ICEM software for dynamic meshing, and the dynamic meshed rotary blade was imported into the EDEM 2018™ software to establish the interaction model of the coupling field. The parameters to be determined for the soil–blade interaction model are shown in Table 1.

TABLE 1. Basic parameters of simulation model.

Parameter	Value
Tillage depth (mm)	80
Density of soil partiel ($\text{kg}\cdot\text{m}^{-3}$)	2150
Density of 65Mn steel ($\text{kg}\cdot\text{m}^{-3}$)	0.3
Poisson's ratio of the soil particles	0.41
Poisson's ratio of 65Mn steel	0.3
Shear modulus of soil partiel (MPa)	1.24×10^6
Shear modulus of 65Mn steel (MPa)	7.9×10^4
Coefficient of restitution between soil and soil	0.6
Coefficient of rolling friction between soil and soil	0.2
Coefficient of static friction between soil and soil	0.3
Coefficient of restitution between soil and 65Mn steel	0.6
Coefficient of rolling friction between soil and 65Mn steel	0.05
Coefficient of static friction between soil and 65Mn steel	0.6
Normal stiffness per unit area ($\text{N}\cdot\text{m}^{-1}$)	3.4×10^8
Shear stiffness per unit area ($\text{N}\cdot\text{m}^{-1}$)	1.5×10^8
Critical Normal stress (Pa)	200,000
Critical Shear stress (Pa)	68,000
Bonded disk radius (mm)	3.5

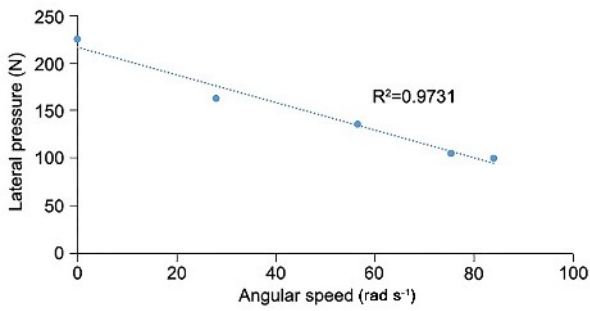
While exploring tillage resistance, the soil–blade model was imported into the Fluent 17.0 module to establish the interaction between the blade and air. The working condition was turbulent, and the RNG $k\text{-}\epsilon$ turbulent flow energy dissipation rate model was used (Ahn et al., 2018; Dai et al., 2022; Huo et al., 2022; Tiwary et al., 2022).

RESULTS AND DISCUSSION

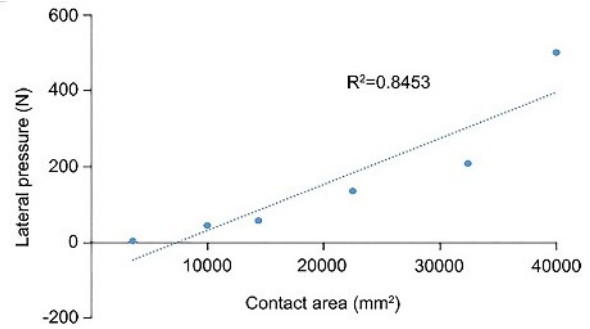
Tillage resistance

Lateral rotational friction

The pressure in the X -axis direction is extracted in the post-processing module, and the collated results are shown in Fig. 4. Based on the simulation results, the lateral pressure of the disc model showed a linear decreasing trend with the increase of angular speed during operation. The fitting equation is shown in [eq. (3)]. The larger the angular speed, the stronger the dynamic effect of the material around the disc model, which dispersed the pressure effect of the material on the part.



a. Lateral pressure varied with angular speed



b. Lateral pressure varied with angular speed

FIGURE 4. Lateral pressure simulation test results.

The lateral pressure showed an increasing trend with the increase in the contact area. The fitting equation is shown in [eq. (4)]. As the contact area increased, the number of materials in contact increased.

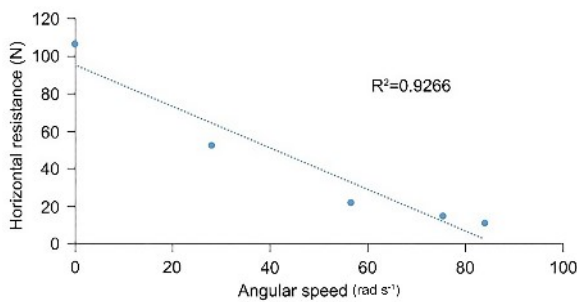
$$X = -1.1078 \omega + 95.251 \tag{3}$$

$$X = 0.0122 A - 90.608 \tag{4}$$

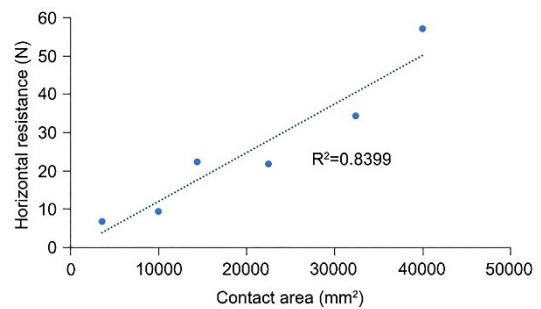
where:

X is the lateral pressure (N),

A is the contact area (mm²).



a. Variation of horizontal resistance with angular speed



b. Variation of horizontal resistance with contact area

FIGURE 5. Horizontal resistance simulation test results.

Horizontal resistance with the increase in contact area showed an increasing trend. The fitting equation is shown in [eq. (6)]. As the contact area increased, the number of materials in contact increased, and the adhesion force between the material and the disc model became greater.

$$Y = -1.1078 \omega + 95.251 \tag{5}$$

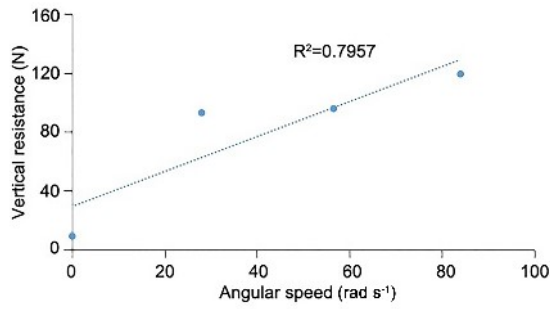
$$Y = 0.0013 A + 0.7685 \tag{6}$$

where:

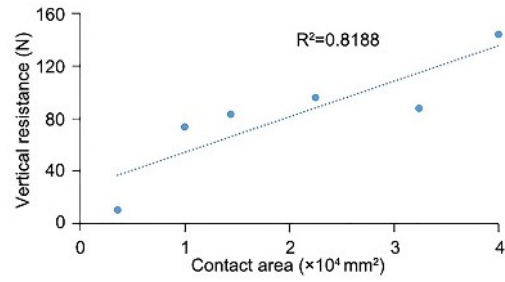
Y denotes the horizontal resistance (N).

The resistance in the Y-axis direction is extracted in the post-processing module, and the collated results are shown in Fig. 5. Based on the simulation results, the horizontal resistance generated by lateral extrusion of the disc model in the operation process showed a linear decreasing trend with the increase in the angular speed. The fitting equation is shown in [eq. (5)]. The larger the angular speed, the weaker the friction between the lateral material and the disc model (changed the friction coefficient), making this situation consistent with the previous literature (Hu et al., 2014).

From the results of vertical resistance can be obtained, shown as Fig. 6. The vertical resistance generated by the lateral extrusion of the disc model in the operation process with the increase in speed was a linear increasing trend. The fitting equation is shown in [eq. (7)]. The greater the angular speed, the stronger the friction between the lateral material and the disc model (which changed the friction coefficient); in this situation, vertical resistance with the increase in contact area showed an increasing trend. The fitting equation is shown in [eq. (8)]. As the contact area increased, the number of materials in contact increased, and the greater the adhesion between the material and the driving soil contact parts.



a. Variation of vertical resistance with angular speed



b. Variation of vertical resistance with angular speed

FIGURE 6. Simulation test results of vertical resistance.

$$Z = 1.19\omega + 29.151 \quad (7)$$

$$Z = 0.0027 A + 26.795 \quad (8)$$

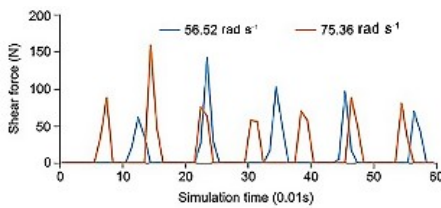
where:

Z is the vertical resistance (N).

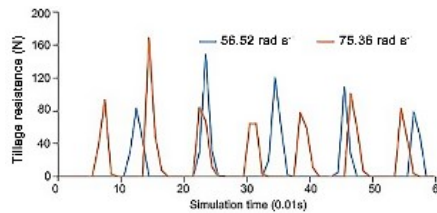
Shear force and tillage resistance

In this model, the average shear force of the cutting edge was 50.88 N at an angular speed of $56.52 \text{ rad}\cdot\text{s}^{-1}$ of the rotary blade, which was lower than 67.96 N at an angular speed of $75.36 \text{ rad}\cdot\text{s}^{-1}$, as shown in Fig. 7a.

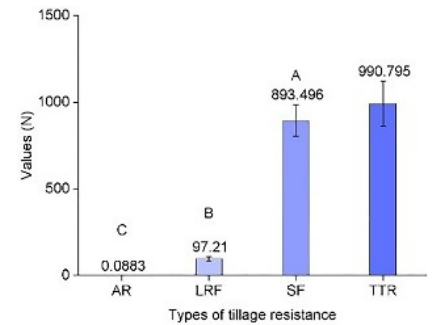
Therefore, increasing the angular speed increased the shear force because the impact between the cutting edge and soil particles was enhanced by increasing the angular speed. When the angular speed was $56.52 \text{ rad}\cdot\text{s}^{-1}$, the average tillage resistance of the rotary blade was 59.46 N, and the shear force accounted for 85.57% of the tillage resistance of the rotary blade. When the angular speed was $75.36 \text{ rad}\cdot\text{s}^{-1}$, the average tillage resistance of the rotary blade was 78.24 N, as shown in Fig. 7b. The shear force accounted for 86.86% of the tillage resistance; therefore, shear force was the main resistance during the operation of the rotary blade.



a. Real-time shear force of rotary blade operating at different angular speeds



b. Real-time tillage resistance of rotary blade operating at different angular speeds



c. Numerical simulation results at $75.36 \text{ rad}\cdot\text{s}^{-1}$

FIGURE 7. Simulation test results of shear force and tillage resistance.

From Fig. 7c, tillage resistance was 990.795 N. When the rotational angular speed of the blade was $75.36 \text{ rad}\cdot\text{s}^{-1}$, air resistance was 0.0883 N, accounting for 0.01% of tillage resistance, which was 7.7% different from the calculation results in section **Air resistance**. The lateral rotational friction was 97.21 N, accounting for 9.81% of tillage resistance, which was different from the sliding friction. The shear force was 893.496 N, accounting for 90.18% of tillage resistance, which was the main

portion of tillage resistance and determined the operating effect of the rotary blade. Therefore, the shape and movement form of the rotary blade edge can be studied to reduce the shear force to reduce the tillage resistance.

Energy consumption

The tillage resistance, torque result output, and power consumption results of the rotary blade operation process in the coupled simulation test were shown in Fig. 8.

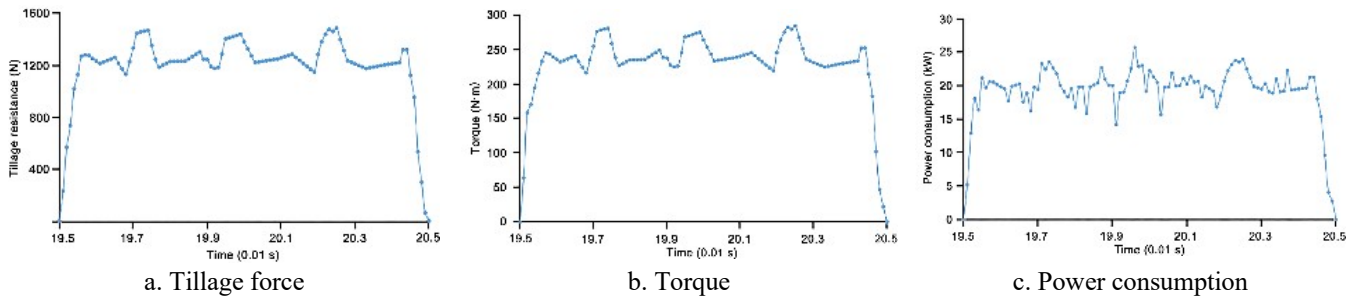


FIGURE 8. Coupling simulation results.

The simulation data of the cut and the left soil bin of the coupled simulation test were excluded, and the output results of the stable operation section of the rotary blade were selected for analysis. The simulation results showed (Fig. 8a and Fig. 8b) that the tillage resistance of plain straight rotary blades in the stable phase was stable in the range of 1100–1500 N, and its torque was stable in the range of 210–285 N·m. The power consumption of the blade in the coupled simulation test was output, and the results are shown in Fig. 8c. The power consumption calculation results showed that the power consumption was in the range of 15.8–24 kW during the stable phase.

Based on the coupled simulation test data, the spatial surface model of tillage resistance, torque, and power consumption was formed, as shown in Fig. 9. Travel speed v and rotation speed n were $0.56 \text{ m}\cdot\text{s}^{-1}$ and 720 rpm, respectively. The model showed that tillage resistance and torque jointly affected power consumption. Power consumption increased with the increase of tillage resistance and torque. The theoretical relationship between power consumption and tillage resistance and

torque was as follows:

$$P = \frac{Fv}{1000} + \frac{Mn}{9550} \tag{9}$$

where:

P is the power consumption of plain straight rotary blades, kW;

F is the tillage resistance of plain straight rotary blades, N,

M is the torque of plain straight rotary blades, N·m.

Fig. 9 shows the theoretical relationship surface, which was a good fit. Only some data points were affected by the coupled simulation environment that was not in the theoretical range, but the overall fit was good. Therefore, the coupled simulation model represented the relationship between tillage resistance, torque, and power consumption more accurately.

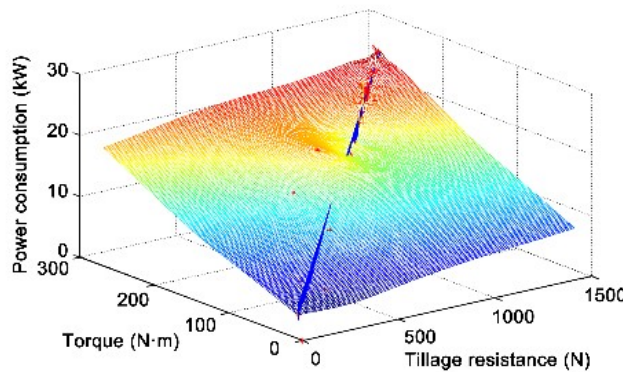


FIGURE 9. Model of tillage resistance and torque on power consumption.

The results of field tests are shown in Fig. 10. The power consumption (range 14 to 30 kW) was less stable compared to the coupled simulation output (range 15.8 to 24 kW), which was due to more instability in the field and therefore resulted in higher fluctuations in the power consumption. The average power consumption of the rotary blade in the field test and the coupled simulation was 22.28 kW and 20.14 kW, respectively. Power consumption in the field test increased by 10.63%

compared to the coupled simulation test, and there was a discrepancy between the two. However, the trend of power consumption in the coupled simulation and field test was basically the same (Fig. 10a), and this variability was within a reasonable range. Yu et al. (2009) and Zhao et al. (2017) also considered the approximate variability acceptable when studying the simulation test, so the coupled airflow–soil–blade simulation model established in this paper was reasonable and simulated rotary blade operation.

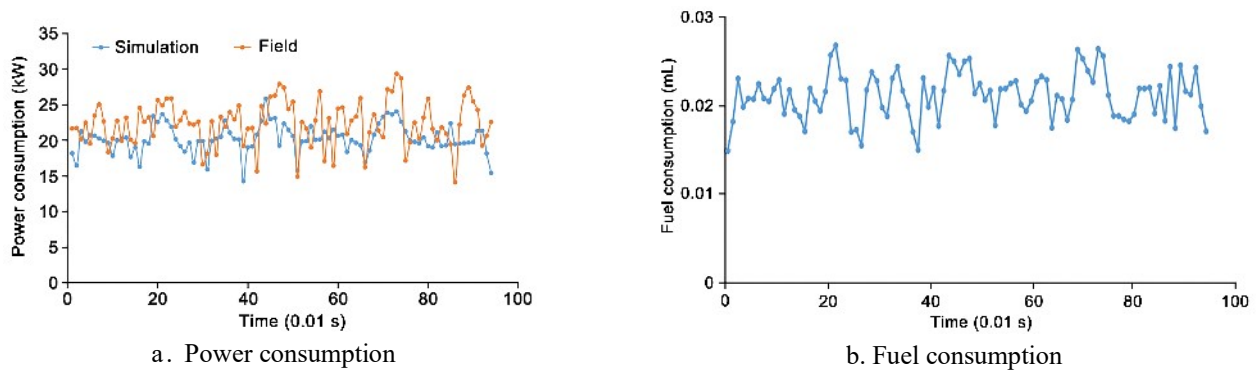


FIGURE 10. Energy consumption and fuel consumption results obtained through field test.

The results of fuel consumption in the field test are shown in Fig. 10b. Since the time interval in the coupled simulation test was 0.01 s, the accumulated time of fuel consumption in the field test needed to be timed and finally processed to the same 0.01 s as the time interval of the

coupled simulation test (i.e., each data point was the oil consumption of a 0.01 s interval). The test results are basically consistent with those measured by Zhao et al. (2015). The modeling of tillage resistance, torque, and fuel consumption was shown in Fig. 11.

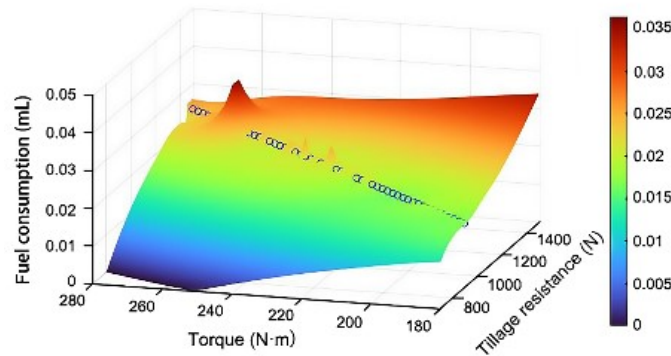


FIGURE 11. Three-dimensional model of torque, tillage resistance and fuel consumption.

The mathematical relationship between tillage resistance and torque on field fuel consumption in the coupled simulation test was as follows:

$$V = p_1 F + p_2 M \quad (10)$$

where:

V is fuel consumption, mL;

p_1 is tillage resistance constant of $1.776 \times 10^{-6} \text{ N} \cdot \text{mL}^{-1}$ for 0.01 s rotary tillage operation,

p_2 is torque constant of $7.88 \times 10^{-5} (\text{N} \cdot \text{m}) \text{ mL}^{-1}$ for 0.01 s rotary tillage operation.

The fit was good, and most of the data points were around this surface. Therefore, this mathematical relationship can be used to represent the relationship between tillage resistance, the torque of rotary blades and the fuel consumption of the field test in the coupled airflow–soil–blade simulation test.

CONCLUSIONS

For the problem of tillage resistance during the operation of plain straight rotary blades, the tillage resistance of the rotary blade was divided into three parts: air resistance, lateral rotation friction resistance, and shear force in this paper.

(1) When the rotary blade was driven by the tractor’s high-grade output shaft to rotate at high speed, the angular speed of the blade was $75.36 \text{ rad} \cdot \text{s}^{-1}$, and the air resistance was 0.0815 N. The coupling simulation output air resistance was 0.0883 N (7.7% difference from the theoretical calculation), and tillage resistance was 990.795 N. Air resistance accounted for 0.01% of tillage resistance. The horizontal resistance generated by lateral extrusion of the rotary blade during operation was linearly decreased with the increase of angular speed and linearly increased with the increase in contact area using discrete element simulation test. Vertical resistance tended to increase linearly with the increase in angular speed and increased linearly with the increase in contact area. The coupling simulation obtained a lateral rotational friction of 97.21 N, accounting for 9.81% of the tillage resistance. The greater the angular speed of the rotary blade, the greater the shear force. The coupling simulation obtained a shear force of 893.496 N, accounting for 90.18% of tillage resistance.

(2) The power consumption and fuel consumption of plain straight rotary tillage operations were tested in the field, and the power consumption ranged from 14 to 30 kW, with an average power consumption of 22.28 kW. Compared with the coupled simulation results, the power consumption increased by 10.63%. The 0.01 s unitisation process was performed on the output of fuel consumption, and the correspondence points were formed with the tillage

resistance and power consumption in the coupled simulation, and the mathematical relationship model of tillage resistance, torque, and fuel consumption was established.

A thorough delineation of tillage resistance and energy consumption will provide theoretical support for the optimal design of rotary blades to reduce resistance and consumption. Meanwhile, the coupled simulation model was established to provide research ideas for the study of the resistance of soil-engaging components.

ACKNOWLEDGEMENTS

This work was financially supported by Technology Support Plan (Grant No.: 2020YFD1000903).

REFERENCES

- Ahmadi I (2017) A torque calculator for rotary tiller using the laws of classical mechanics. *Soil and Tillage Research* 165: 137-143. <https://doi.org/10.1016/j.still.2016.08.009>
- Ahmadi I (2018) A draught force estimator for disc harrow using the laws of classical soil mechanics. *Biosystems Engineering* 171: 52-62. <https://doi.org/10.1016/j.biosystemseng.2018.04.008>
- Ahn S-H, Xiao YX, Wang ZW, Luo YY, Fan HG (2018) Unsteady prediction of cavitating flow around a three dimensional hydrofoil by using a modified RNG k- ϵ model. *Ocean Engineering* 158: 275-285. <https://doi.org/10.1016/j.oceaneng.2018.04.005>
- Aleshin V, Van Den Abeele K (2009) Preisach analysis of the Hertz–Mindlin system. *Journal of the Mechanics and Physics of Solids* 57(4): 657-672. <https://doi.org/10.1016/j.jmps.2009.01.004>
- Al-Janobi A (2000) A data-acquisition system to monitor performance of fully mounted implements. *Journal of Agricultural Engineering Research* 75(2): 167-175. <https://doi.org/10.1006/jaer.1999.0496>
- Asl JH, Singh S (2009) Optimization and evaluation of rotary tiller blades: computer solution of mathematical relations. *Soil and Tillage Research* 106(1): 1-7. <https://doi.org/10.1016/j.still.2009.09.011>
- Azimi-Nejadian H, Karparvarfard SH, Naderi-Boldaji M (2022) Weed seed burial as affected by mouldboard design parameters, ploughing depth and speed: DEM simulations and experimental validation. *Biosystems Engineering* 216: 79-92. <https://doi.org/10.1016/j.biosystemseng.2022.02.005>
- Billy M de, Cohen Tenoudji F (2021) Resonance ultrasonic spectroscopy applied to normal and tangential contact modes investigation of a constrained metallic sphere. *Ultrasonics* 117: 106539. <https://doi.org/10.1016/j.ultras.2021.106539>
- Celik A, Altikat S, Way TR (2013) Strip tillage width effects on sunflower seed emergence and yield. *Soil and Tillage Research* 131: 20-27. <https://doi.org/10.1016/j.still.2013.03.004>
- Chen PY, Han YL, Jia FG, Zhao D, Meng XY, Li AQ, Chu YH, Zhao HW (2022) Investigation of the mechanism of aerodynamic separation of rice husks from brown rice following paddy hulling by coupled CFD-DEM. *Biosystems Engineering* 218: 200-215. <https://doi.org/10.1016/j.biosystemseng.2022.03.015>
- Chertkiattipol S, Niyamapa T (2010) Variations of torque and specific tilling energy for different rotary blades. *International Agricultural Engineering Journal* 19(3): 1-14.
- Dai T, Liu SM, Liu JJ, Jiang N, Liu W, Chen QY (2022) Evaluation of fast fluid dynamics with different turbulence models for predicting outdoor airflow and pollutant dispersion. *Sustainable Cities and Society* 77: 103583. <https://doi.org/10.1016/j.scs.2021.103583>
- Foley AG, Lawton PJ, Barker AW, McLees VA (1984) The use of alumina ceramic to reduce wear of soil-engaging components. *Journal of Agricultural Engineering Research* 30: 37-46. [https://doi.org/10.1016/S0021-8634\(84\)80004-9](https://doi.org/10.1016/S0021-8634(84)80004-9)
- Guan CS, Fu JJ, Cui ZC, Wang SL, Gao QS, Yang YT (2021) Evaluation of the tribological and anti-adhesive properties of different materials coated rotary tillage blades. *Soil and Tillage Research* 209: 104933. <https://doi.org/10.1016/j.still.2021.104933>
- Guan CS, Fu JJ, Xu L, Jiang XZ, Wang SL, Cui ZC (2022) Study on the reduction of soil adhesion and tillage force of bionic cutter teeth in secondary soil crushing. *Biosystems Engineering* 213: 133-147. <https://doi.org/10.1016/j.biosystemseng.2021.11.018>
- Hu JP, Zhou CJ, Hou C, Wang J (2014) Simulation analysis of seed-filling performance of magnetic plate seed-metering device by discrete element method. *Transactions of the Chinese Society for Agricultural Machinery* 45(2): 94-98. <https://doi.org/10.6041/j.issn.1000-1298.2014.02.016>
- Huo J, Wang Z, Luan X, Jing M, Hou S, Jiang J, Zhang B (2022) The CFD modeling of bund overtopping phenomena and prediction of dynamic pressure on the bund. *Journal of Loss Prevention in the Process Industries* 74: 104653. <https://doi.org/10.1016/j.jlpi.2021.104653>
- Kasisira LL, du Plessis HLM (2006) Energy optimization for subsoilers in tandem in a sandy clay loam soil. *Soil and Tillage Research* 86(2): 185-198. <https://doi.org/10.1016/j.still.2005.02.031>
- Kichler CM, Fulton JP, Raper RL, McDonald TP, Zech WC (2011) Effects of transmission gear selection on tractor performance and fuel costs during deep tillage operations. *Soil and Tillage Research* 113(2): 105-111. <https://doi.org/10.1016/j.still.2011.03.002>
- Kogut Z, Sergiel L, Żurek G (2016) The effect of the disc setup angles and working depth on disc harrow working resistance. *Biosystems Engineering* 151: 328-337. <https://doi.org/10.1016/j.biosystemseng.2016.10.004>
- Kong XR, Liu J, Yang TY, Su YC, Geng J, Niu ZY (2022) Numerical simulation of feed pellet breakage in pneumatic conveying. *Biosystems Engineering* 218: 31-42. <https://doi.org/10.1016/j.biosystemseng.2022.03.012>

- Kravchenko K, Hauser V, Gorbunov M (2019) Estimating the brake disc air resistance by scaled test rig and by computer simulation. *Transportation Research Procedia* 40: 737-744. <https://doi.org/10.1016/j.trpro.2019.07.104>
- Laufer D, Koch H-J (2017) Growth and yield formation of sugar beet (*Beta vulgaris* L.) under strip tillage compared to full width tillage on silt loam soil in Central Europe. *European Journal of Agronomy* 82: 182-189. <https://doi.org/10.1016/j.eja.2016.10.017>
- Lee S-y, Lee I-b, Yeo U-h, Kim J-g, Kim R-w, Kwon K-s (2022) Dynamic energy model of a naturally ventilated duck house and comparative analysis of energy loads according to ventilation type. *Biosystems Engineering* 219: 218-234. <https://doi.org/10.1016/j.biosystemseng.2022.05.003>
- Li B, Liu FY, Mu JY, Chen J, Han WT (2014) Distinct element method analysis and field experiment of soil resistance applied on the subsoiler. *International Journal of Agricultural and Biological Engineering* 7(1): 1-6. <https://doi.org/10.3965/j.ijabe.20140701.006>
- Licht MA, Al-Kaisi M (2005) Strip-tillage effect on seedbed soil temperature and other soil physical properties. *Soil and Tillage Research* 80(1): 233-249. <https://doi.org/10.1016/j.still.2004.03.017>
- Lowry CJ, Robertson GP, Brainard DC (2021) Strip-tillage decreases soil nitrogen availability and increases the potential for N losses in a cover cropped organic system. *Agriculture, Ecosystems & Environment* 319: 107524. <https://doi.org/10.1016/j.agee.2021.107524>
- Luna JM, Staben ML (2002) Strip tillage for sweet corn production: yield and economic return. *HortScience* 37(7): 1040-1044. <https://doi.org/10.21273/HORTSCI.37.7.1040>
- Mak J, Chen Y (2015) Simulation of draft forces of a sweep in a loamy sand soil using the discrete element method. *Canadian Biosystems Engineering* 56(1): 2.1-2.7. <https://doi.org/10.7451/CBE.2014.56.2.1>
- Matin MA, Desbiolles JMA, Fielke JM (2016) Strip-tillage using rotating straight blades: Effect of cutting edge geometry on furrow parameters. *Soil and Tillage Research* 155: 271-279. <https://doi.org/10.1016/j.still.2015.08.016>
- Matin MA, Fielke JM, Desbiolles JMA (2014) Furrow parameters in rotary strip-tillage: Effect of blade geometry and rotary speed. *Biosystems Engineering* 118: 7-15. <https://doi.org/10.1016/j.biosystemseng.2013.10.015>
- Matin MA, Fielke JM, Desbiolles JMA (2015) Torque and energy characteristics for strip-tillage cultivation when cutting furrows using three designs of rotary blade. *Biosystems Engineering* 129: 329-340. <https://doi.org/10.1016/j.biosystemseng.2014.11.008>
- Matin MA, Hossain MI, Gathala MK, Timsina J, Krupnik TJ (2021) Optimal design and setting of rotary strip-tiller blades to intensify dry season cropping in Asian wet clay soil conditions. *Soil and Tillage Research* 207: 104854. <https://doi.org/10.1016/j.still.2020.104854>
- McKyes E, Desir FL (1984) Prediction and field measurements of tillage tool draft forces and efficiency in cohesive soils. *Soil and Tillage Research* 4(5): 459-470. [https://doi.org/10.1016/0167-1987\(84\)90053-9](https://doi.org/10.1016/0167-1987(84)90053-9)
- Reece AR (1965) Paper 2: The fundamental equation of earth-moving mechanics. *Proceedings of the Institution of Mechanical Engineers, Conference Proceedings* 179(6): 16-22. https://doi.org/10.1243/PIME_CONF_1964_179_134_02
- Sahu RK, Raheman H (2006) Draught prediction of agricultural implements using reference tillage tools in sandy clay loam soil. *Biosystems Engineering* 94(2): 275-284. <https://doi.org/10.1016/j.biosystemseng.2006.01.015>
- Saimbhi VS, Wadhwa DS, Grewal PS (2004) Development of a rotary tiller blade using three-dimensional computer graphics. *Biosystems Engineering* 89(1): 47-58. <https://doi.org/10.1016/j.biosystemseng.2004.05.011>
- Sakai M, Koshizuka S (2009) Large-scale discrete element modeling in pneumatic conveying. *Chemical Engineering Science* 64(3): 533-539. <https://doi.org/10.1016/j.ces.2008.10.003>
- Serrano JM, Peça JO, Marques da Silva J, Pinheiro A, Carvalho M (2007) Tractor energy requirements in disc harrow systems. *Biosystems Engineering* 98(3): 286-296. <https://doi.org/10.1016/j.biosystemseng.2007.08.002>
- Serrano JM, Peça JO, Pinheiro A, Carvalho M, Nunes M, Ribeiro L, Santos F (2003) The effect of gang angle of offset disc harrows on soil tillth, work rate and fuel consumption. *Biosystems Engineering* 84(2): 171-176. [https://doi.org/10.1016/S1537-5110\(02\)00261-1](https://doi.org/10.1016/S1537-5110(02)00261-1)
- Shahgoli G, Fielke J, Saunders C, Desbiolles J (2010) Simulation of the dynamic behaviour of a tractor-oscillating subsoiler system. *Biosystems Engineering* 106(2): 147-155. <https://doi.org/10.1016/j.biosystemseng.2010.03.002>
- Shahgoli G, Saunders C, Desbiolles J, Fielke J (2009) The effect of oscillation angle on the performance of oscillatory tillage. *Soil and Tillage Research* 104(1): 97-105. <https://doi.org/10.1016/j.still.2009.01.003>
- Shaikh SA, Li Y, Ma Z, Chandio FA, Tunio MH, Liang Z, Solangi KA (2021) Discrete element method (DEM) simulation of single grouser shoe-soil interaction at varied moisture contents. *Computers and Electronics in Agriculture* 191: 106538. <https://doi.org/10.1016/j.compag.2021.106538>

- Su Z, Li YM, Dong YH, Tang Z, Liang ZW (2020) Simulation of rice threshing performance with concentric and non-concentric threshing gaps. *Biosystems Engineering* 197: 270-284. <https://doi.org/10.1016/j.biosystemseng.2020.05.020>
- Teitel M, Ozer S, Mendelovich V (2022) Airflow temperature and humidity patterns in a screenhouse with a flat insect-proof screen roof and impermeable sloping walls-Computational fluid dynamics (CFD) results. *Biosystems Engineering* 214: 165-176. <https://doi.org/10.1016/j.biosystemseng.2020.05.020>
- Tiwary B, Kumar R, Singh PK (2022) Thermofluidic characteristic of a nanofluid-cooled oblique fin heat sink: an experimental and numerical investigation. *International Journal of Thermal Sciences* 171: 107214. <https://doi.org/10.1016/j.ijthermalsci.2021.107214>
- Tong J, Ji WF, Jia HL, Chen DH, Yang XW (2015) Design and tests of biomimetic blades for soil-rototilling and stubble-breaking. *Journal of Bionic Engineering* 12(3): 495-503. [https://doi.org/10.1016/S1672-6529\(14\)60140-2](https://doi.org/10.1016/S1672-6529(14)60140-2)
- Turmel M-S, Speratti A, Baudron F, Verhulst N, Govaerts B (2015) Crop residue management and soil health: A systems analysis. *Agricultural Systems* 134: 6-16. <https://doi.org/10.1016/j.agsy.2014.05.009>
- USDA - United States Department of Agriculture (1993) Soil survey manual. USDA, Handbook n.18.
- Vaitauskienė K, Šrauskis E, Romanekas K, Jasinskas A (2017) Design, development and field evaluation of row-cleaners for strip tillage in conservation farming. *Soil and Tillage Research* 174: 139-146. <https://doi.org/10.1016/j.still.2017.07.006>
- Wang N, Yang SQ, Zhao TT, Cao B, Wang CW (2020) Amending research on the expression of the contact force of the spindle barrel finishing based on EDEM simulation. *Chinese Journal of Mechanical Engineering* 33(6): 83. <https://doi.org/10.1186/s10033-020-00502-x>
- Wang XZ, Zhang S, Pan HB, Zheng ZQ, Huang YX, Zhu RX (2019) Effect of soil particle size on soil-subsoiler interactions using the discrete element method simulations. *Biosystems Engineering* 182: 138-150. <https://doi.org/10.1016/j.biosystemseng.2019.04.005>
- Yang YW, Li M, Tong J, Ma YH (2018) Study on the interaction between soil and the five-claw combination of a mole using the discrete element method. *Applied Bionics and Biomechanics* 2018: 7854052. <https://doi.org/10.1155/2018/7854052>
- Yu JQ, Qian LS, Yu WJ, Pan SQ, Fang Y, Fu H (2009) DEM analysis of the resistances applied on furrow openers. *Transactions of the Chinese Society for Agricultural Machinery* 40(6): 53-57. <https://doi.org/10.3969/j.issn.1000-1298>
- Zhang J, Kushwaha RL (1995) A modified model to predict soil cutting resistance. *Soil and Tillage Research* 34(3): 157-168. [https://doi.org/10.1016/0167-1987\(95\)00466-6](https://doi.org/10.1016/0167-1987(95)00466-6)
- Zhang JB, Tong J, Ma YH (2014) Design and experiment of bionic anti-drag subsoiler. *Transactions of the Chinese Society for Agricultural Machinery* 45(4): 141-145. <https://doi.org/10.6041/j.issn.1000-1298.2014.04.022>
- Zhang SX, Chen XW, Jia SX, Liang AZ, Zhang XP, Yang XM, Wei SC, Sun BJ, Huang DD, Zhou GY (2015) The potential mechanism of long-term conservation tillage effects on maize yield in the black soil of Northeast China. *Soil and Tillage Research* 154: 84-90. <https://doi.org/10.1016/j.still.2015.06.002>
- Zhao D, Li Li, Xu C, Qi X, Li X, Li M (2015) Prediction model of fuel consumption with single working part for front-stubble-breaking and front-subsoil combined cultivating machine based on the influence of tiller depth. *Acta Agriculturae Boreali-occidentalis Sinica* 24(6):171-178. <https://doi.org/10.7606/j.issn.1004-1389.2015.06.027>
- Zhao MQ, Liu YQ, Hu YW (2012) An airflow field finite element analysis of the seed adsorption hole of pneumatic seeder. *Applied Mechanics Materials* 117-119: 1810-1815. <https://doi.org/10.4028/www.scientific.net/AMM.117-119.1810>
- Zhao SH, Liu HJ, Tan HW, Cao XZ, Zhang XM, Yang YQ (2017) Design and performance experiment of opener based on bionic sailfish head curve. *Transactions of the Chinese Society of Agricultural Engineering* 33(5): 32-39. <https://doi.org/10.11975/j.issn.1002-6819.2017.05.005>